Understanding adsorption and desorption processes in mesoporous materials with independent disordered channels

Sergej Naumov, Rustem Valiullin,* and Jörg Kärger
Fakultät für Physik und Geowissenschaften, Univerität Leipzig, D-04103 Leipzig, Germany

Peter A. Monson
Department of Chemical Engineering, University of Massachusetts, Amherst, Massachusetts 01003, USA

Using a lattice-gas model in mean-field theory, we discuss the problem of how adsorption and desorption of fluids in independent cylinderlike pores is influenced by variations in the pore diameter along the length of the pore, surface roughness of the pore walls, and chemical heterogeneity. We also consider the impact of contact with the bulk phase via the pore opening and the possibility of interactions between neighboring pores via a liquid film on the external surface of the material. We find that a combination of pore size variation along the length of the pore and surface roughness yields sorption hysteresis similar to that found in systems with three-dimensional disordered pore networks such as porous glasses. Our results are especially relevant to adsorption and desorption in porous silicon materials with independent linear pores and apparently anomalous features of the behavior in these systems can be accounted for within the context of the present model.

I. INTRODUCTION

Adsorption of gases by mesoporous materials at subcritical temperatures is often accompanied by hysteresis, i.e., the amount adsorbed depends on whether the gas pressure of the surrounding atmosphere is increased (adsorption branch) or decreased (desorption branch). Such behavior is generally associated with confinement effects upon condensation and evaporation transitions occurring in pores. In addition to shifts of the transition pressures as compared to the bulk one, variation in pore sizes within a material may lead to evaporation or condensation occurring over a range of pressures. In the simplest way, this may be governed by the distribution of the pore sizes. It has already long ago been noted [1] that for an array of independent pores with different pore sizes, both desorption and adsorption branches should be affected in the same way, i.e., these two branches should be parallel to each other (according to IUPAC, these types of isotherms are referred to as of type H1 [2]). Experiments, however, often reveal asymmetric hysteresis loops (H2-type). This is typically the case for materials with highly networked pore structures, such as random porous glasses, and the asymmetry of the hysteresis is generally considered as a consequence of interconnectivity of the pores [3,4].

Despite many experimental studies devoted to the understanding of the relationship between pore geometry and sorption behavior, limited possibilities for a control over the pore structure precluded definitive answers. The advent of template-based mesoporous materials was expected to substantially contribute to a more clearly defined assessment of theoretical predictions. However, it has become evident that the experimental results obtained using these materials still may suffer from some "nonideality" effects. These include, first of all, the occurrence of some defects in their structure

[5], such as the existence of interconnections between individual channels (known, e.g., for SBA-15 material). Another type of complications may arise from finite-size effects. For example, length of individual MCM-41 channels does typically not exceed about 100 nm. This may have some effect on the sorption behavior.

Recently, porous silicon (PSi) materials, obtained using electrochemical etching of single crystals, have emerged as promising potential candidates for studying the effects of pore structure on phase equilibria in pores. It has been shown that by proper tuning of the fabrication conditions, PSi with independent linear pores up to a few hundred micrometers in length can be obtained [6]. A number of different experimental methods have been used to verify the absence of the intersections between individual channels [7,8]. Importantly, the fabrication procedure also allows some control of the shape of the pores [9–11]. Given such attractive options for structural control, PSi has been extensively used for experimental studies [7,10,12–17]. However, the experiments revealed some unexpected, apparently, counterintuitive results.

In the process of electrochemical fabrication of PSi, a porous film is grown on a silicon substrate. This provides a simple means to prepare channel-like pores open at both ends (upon detaching the porous film from the substrate by the use of an electropolishing current pulse) or only at one end (leaving the porous film on the substrate). These two materials have potential to reveal insights into the nature of the capillary condensation processes in independent pores. In the pioneering approach developed by Cohan in 1938 [18], the adsorption hysteresis in a cylindrical pore open at both ends is due to the difference in the shape of the vapor-liquid menisci appearing on adsorption (cylindrical meniscus) and desorption (hemispherical meniscus). Thus, according to the Kelvin equation, the respective transition pressures will be shifted with respect to each other. Since closing one end of the pore removes the difference in the menisci shape, it should also remove the hysteresis. The experiments with PSi, however, have shown identical adsorption isotherms irre-

---

*Author to whom correspondence should be addressed. valiullin@uni-leipzig.de

spective of whether the pores are open at both ends or just one end [8,19]. Based on this finding, it is natural to question the applicability of the Cohan picture to PSi.

The second interesting observation was that PSi exhibit H2-type hysteresis, although the individual channels are isolated from each other. Generally, hysteresis loops of type H2 are believed to result from pore network effects. These effects can be modeled theoretically using pore blocking or percolation concepts [3] or by using statistical mechanical models of adsorption in complex disordered pore structures [20,21]. In addition to such an asymmetry, the network effects result in a specific types of the so-called desorption and adsorption scanning curves [1,22,23]. Scanning curves typical of interconnected structures have also been found for PSi [14]. Keeping in mind the assumed tubular pore geometry in PSi materials without intersections between individual channels, rationalizing all these experimental results would seem to depend on hypothesizing some kind of interpore interactions leading to cooperative evaporation processes from the pores. As one of the possible mechanisms of such an interaction, the existence of a liquid film on the external surface of PSi has been suggested [14].

Wallacher *et al.* performed adsorption experiments with PSi with an ink-bottle morphology of the pores [10]. Interestingly, they found apparently identical hysteresis behaviors irrespective of whether the bottle part of the PSi channels had direct contact to the gas phase or only through the narrow neck. That means that in the latter case, the larger pores emptied even if the necks remained filled with liquid. Although such behavior, i.e., evaporation via the cavitation process is known to occur under certain conditions [24–26], the difference Δd in the diameters of bottle and neck parts in [10] of about only 1 nm was too small to support this scenario. In addition, the authors found very slow density relaxation in the hysteresis region, which followed stretched-exponential form with a stretching exponent less than one. This has been attributed to the effects of quenched disorder on the length scale below Δd, which, subsequently, has been anticipated to account for the identical hysteresis behaviors for two different pore geometries.

In light of such challenging experimental results, recently we have performed a study using mean-field theory (MFT) of a lattice gas of how disorder in linear pores may affect sorption behavior [8]. It was found that all the experimental findings described above can be uniformly explained taking account of strong disorder of the pore diameter. The main goal of the present paper is to provide more detailed information about the influence of different types of disorder (geometrical and chemical) in these systems as described by the MFT calculations.

II. METHOD

A. Lattice-gas model and mean-field theory

Lattice-gas models have been shown to be a powerful approach for the description of the confined fluids [20,27–31]. The application of the MFT to the lattice model was shown to be especially helpful in elucidating the nature of the adsorption hysteresis for fluids confined in a mesopo-

rous matrix [20,21,32,33]. This approach allows a very efficient calculation of the fluid states depending on the external conditions given by, e.g., chemical potential or temperature, making the static MFT a suitable tool for studying the metastable configurations and phase transitions. In this section, we give a short overview of this method. Further details may be found in [32].

The Hamiltonian of a lattice-gas system with only nearest-neighbor interaction considered is given by

$$\mathcal{H} = -\frac{\epsilon}{2} \sum_{\mathbf{i}} \sum_{\mathbf{a}} n_{\mathbf{i}} n_{\mathbf{i}+\mathbf{a}} + \sum_{\mathbf{i}} n_{\mathbf{i}} \phi_{\mathbf{i}}, \tag{1}$$

where ϵ denotes the nearest-neighbor interaction strength, $\mathbf{i}$ denotes a set of lattice coordinates, $\mathbf{a}$ denotes the vector to a nearest-neighbor site, and $n_{\mathbf{i}}$ is the occupancy at site $\mathbf{i}$. The external field $\phi_{\mathbf{i}}$ at site $\mathbf{i}$ is a nearest-neighbor attraction of strength $y\epsilon$. In terms of the local fluid density $0 \leq \rho_{\mathbf{i}} \leq 1$, the grand free energy Ω for such a system in mean-field theory can be expressed as

$$\Omega = kT \sum_{\mathbf{i}} \left[\rho_{\mathbf{i}} \ln \rho_{\mathbf{i}} + (1 - \rho_{\mathbf{i}}) \ln(1 - \rho_{\mathbf{i}}) \right] - \frac{\epsilon}{2} \sum_{\mathbf{i}} \sum_{\mathbf{a}} \rho_{\mathbf{i}} \rho_{\mathbf{i}+\mathbf{a}} + \sum_{\mathbf{i}} \rho_{\mathbf{i}} [\phi_{\mathbf{i}} - \mu], \tag{2}$$

where μ is the chemical potential, which is uniform everywhere in the system at the equilibrium. The necessary condition for a minimum of Ω is

$$\frac{\partial \Omega}{\partial \rho_{\mathbf{i}}} = 0 \quad \forall \, \mathbf{i}. \tag{3}$$

Using Eqs. (2) and (3), we obtain

$$kT \ln \left[\frac{\rho_{\mathbf{i}}}{1 - \rho_{\mathbf{i}}} \right] - \epsilon \sum_{\mathbf{a}} \rho_{\mathbf{i}+\mathbf{a}} + \phi_{\mathbf{i}} - \mu = 0 \quad \forall \, \mathbf{i}. \tag{4}$$

This can be rearranged into the following expression for $\rho_{\mathbf{i}}$ suitable for iteration:

$$\rho_{\mathbf{i}} = \frac{1}{1 + \exp\left[-\left(\epsilon \sum_{\mathbf{a}} \rho_{\mathbf{i}+\mathbf{a}} - \phi_{\mathbf{i}} + \mu \right) \middle/ kT \right]} \quad \forall \, \mathbf{i}. \tag{5}$$

B. Pore model

In our calculations, we consider a pore composed of a random set of slit pore segments arranged along the x axis and infinitely extended in y direction (Fig. 1). This is the
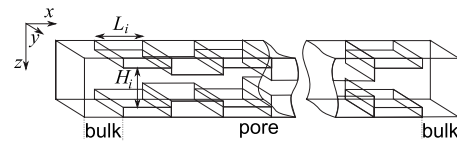
FIG. 1. Schematic representation of a pore consisting of slit segments with varying height H_i along the x axis and constant length L. The pore is infinitely extended in the y direction.
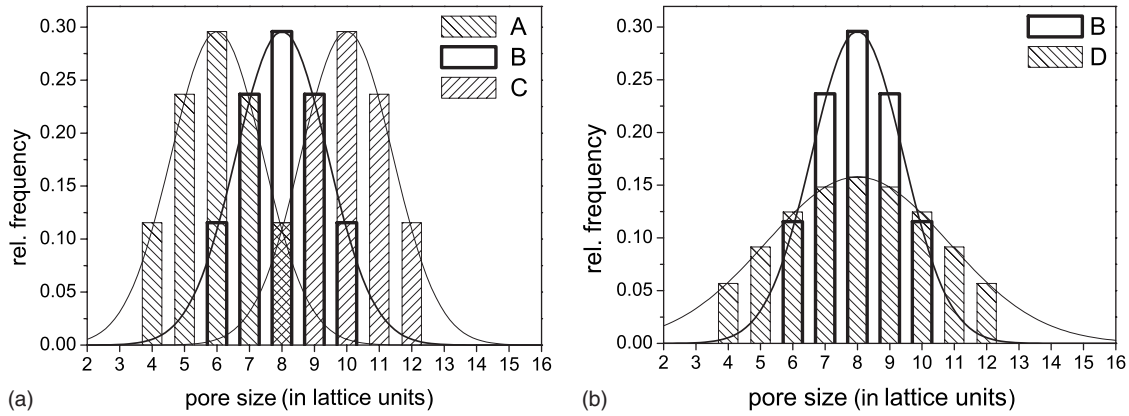
FIG. 2. Pore size distributions studied. Pore size (in lattice units) A, 4–8; B, 6–10; C, 8–12; and D, 4–12. The lines are a guide for the eyes.

simplest model of isolated pores with disorder. The density is independent of y direction [32]. This geometry has similar behavior to the cylindrical pore (as can be seen by comparing the results in [34] for cylindrical pores with those in [35] for slit pores), but rendering the problem two dimensional saves computer time. The height of the pore H_i is varied randomly for each segment in such a way that the overall pore size distribution (PSD) has a Gaussian shape (Fig. 2). Periodic boundary conditions are applied in the x and z directions. For the lattice sites occupied by pore walls and, thus, not accessible to fluid, the boundary conditions for z direction have no influence. The total length of the pore L is the sum of single segment lengths L_i. At each end of the system, we have contact with the bulk lattice gas, which occupies a total length of ten lattice sites each.

In the present work, we have considered three types of disorder. (i) Pore size disorder, which is modeled by the variation in the pore width H_i along the channel direction. We fixed the segment length L_i to ten lattice sites (variation in the segment length does not affect the qualitative behavior) and the pore had 500 segments. The visualization of such a disorder is nicely seen in, e.g., Fig. 3. (ii) The geometrical roughness of the pore wall, which is modeled by randomly adding up to ten single solid sites on the surface of a segment. In order to keep the pore volume constant, simultaneously one wall site is removed from the surface next to each site added. This roughness slightly changes the PSD
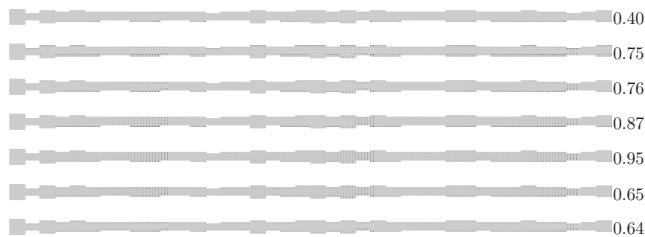
making it wider, but the mean pore size remains constant (Fig. 4). (iii) The chemical heterogeneity of the surface, which can be modeled by a local variation in the solid-fluid interaction parameter y. Figure 5 shows the fluid states in a pore with a surface field variation corresponding to the surface field as created by the geometrical pore wall roughness.

To test the influence of the pore size and its inhomogeneity, we considered four different realizations with Gaussian PSDs: A-with segment pore size from 4 to 8 lattice units; B-6 to 10 lattice units; C-8 to 12 lattice units; and D-4 to 12 lattice units. The PSDs for A, B, and C have the same shape [Fig. 2(a)] but shifted toward the higher mean value. The PSDs for B and D have different widths, but the same mean value of 8 lattice units [Fig. 2(b)].

All calculations have been performed at $T^*=kT/\epsilon=1$, which is 2/3 of the bulk critical temperature for the simple-cubic lattice gas in MFT. For comparison, nitrogen at 77 K is at about 61% of its bulk critical temperature. The fluid density profiles are presented by representing the lattice sites as squares and shading them in grayscale so that white corresponds to zero average occupancy and black to unit average occupancy. The adsorption and desorption isotherms were calculated for a single pore with 500 segments. Averaging over many random realizations (i.e., random array of segments with same PSD) keeping the PSD constant, does not change the qualitative picture of the isotherms. The adsorption and/or desorption isotherms are plotted as average occupancy versus the relative activity $z=\lambda/\lambda_0 \propto P/P_0$, where λ

FIG. 3. Visualizations of fluid density states in the channel A without geometrical roughness. The sequence of states corresponds to adsorption followed by desorption from top to bottom. The z values are given to the right of the images. The first 40 segments of the pore are shown with the pore opening and bulk region on the left.
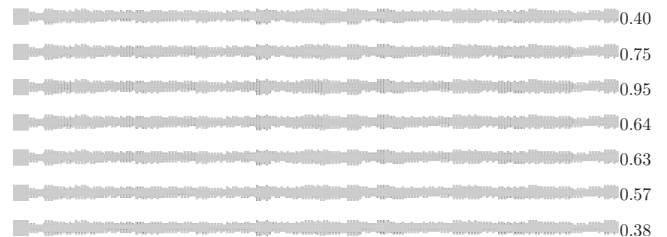
FIG. 4. Visualizations of fluid density states in the channel A with geometrical roughness. The sequence of states corresponds to adsorption followed by desorption from top to bottom. The z values are given to the right of the images. The first 40 segments of the pore are shown with the pore opening and bulk region on the left.
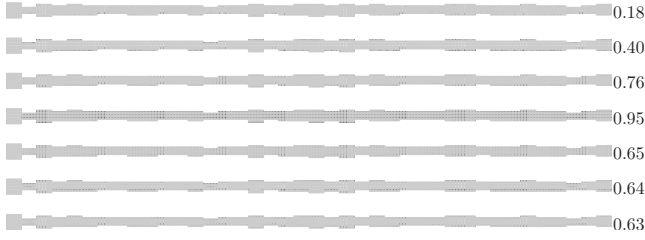
FIG. 5. Visualizations of fluid density states in the channel A with chemical heterogeneity corresponding to geometrical roughness. The sequence of states corresponds to adsorption followed by desorption from top to bottom. The z values are given to the right of the images. The first 40 segments of the pore are shown with the pore opening and bulk region on the left.

$=\exp(\mu/kT)$ and the 0 subscript denotes the value at bulk saturation (the difference between z and P/P_0 reflects the small gas imperfection in bulk at these conditions).

III. RESULTS

A. Effect of pore size disorder

We first consider the influence of the pore size disorder on the adsorption and/or desorption behavior in a single channel, as characterized by a variation in the segment width H_i along the pore. In Fig. 6, we show the adsorption and de-

sorption isotherms for the four different pore size distributions shown in Fig. 2 and for the three types of pore surfaces, i.e., homogeneous surface, geometrically heterogeneous surface, and chemically heterogeneous surface. For the case of a flat homogeneous surface (solid line) for the A-type channel [Fig. 6(a)], we observe a sharp increase in the amount adsorbed at $z \approx 0.35$ for $y=2$. This step reflects the formation of a monolayer on the pore wall surface (as visualized in Fig. 3 for $z=0.40$). Further uptake in the A-type channel is controlled by multilayer adsorption and by capillary condensation in the segments in the order of the increasing segment size H_i. This can be recognized from the visualizations of the fluid density profiles in Fig. 3 for $z \geq 0.76$ and is reflected by steep jumps in the adsorption isotherm [Fig. 6(a)]. After the pores are filled completely, the desorption first occur by the decrease in liquid density in the pore, i.e., by stretching of liquid. Figure 3 shows a visualization of this state ($z=0.65$), where one may see the liquid state with the lower density represented by a lighter gray color.

The question of whether pore blocking [36–38] or cavitation of the liquid [24,34] controls the desorption process can be elucidated by comparing the desorption isotherms for the finite and infinitely long channels. In the latter case, the cavitation process (in MFT) will occur when the stability limit of the liquid is reached. The infinite pore can be modeled by removing the bulk regions but maintaining the periodic boundaries in the x direction. In Fig. 7, the adsorption and desorption isotherms for the A- and B-type pores with homo-
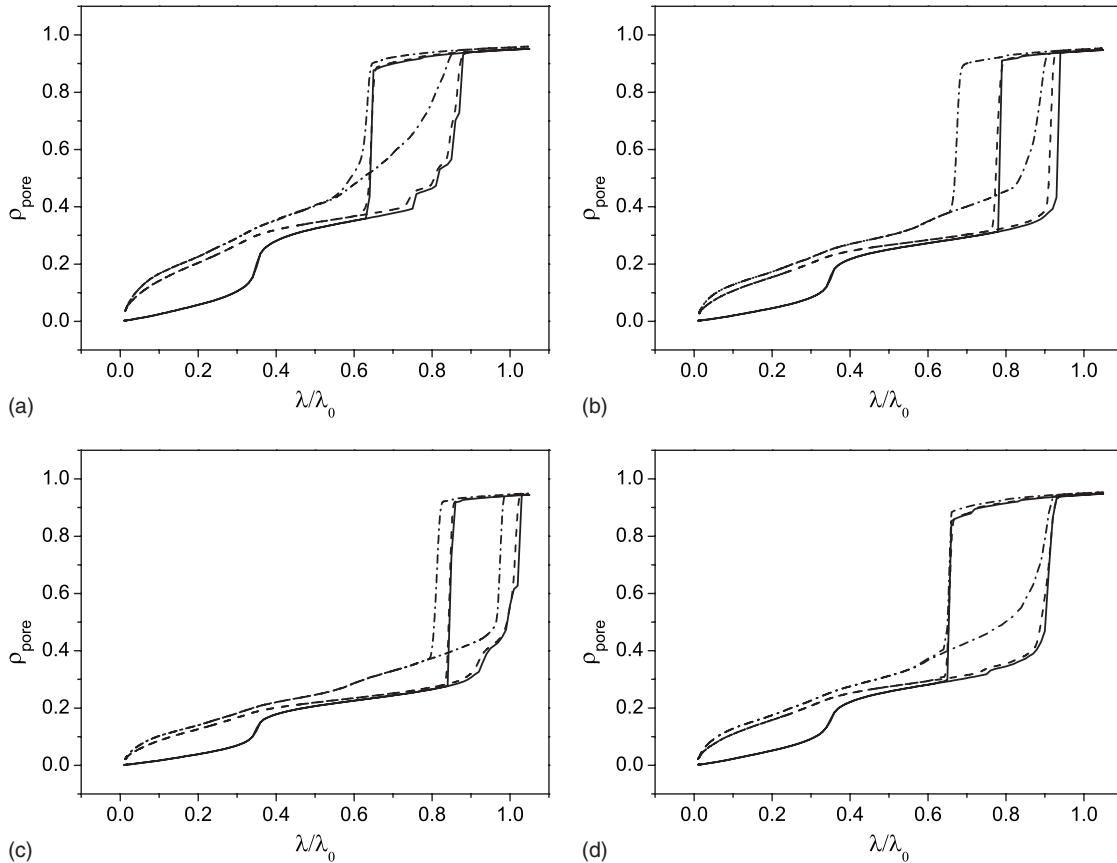
FIG. 6. Adsorption and desorption isotherms calculated for systems with PSDs A, B, C, and D, respectively. The solid lines: isotherms for flat surface, dot-dashed lines: rough surface, and dashed lines: chemical heterogeneity.
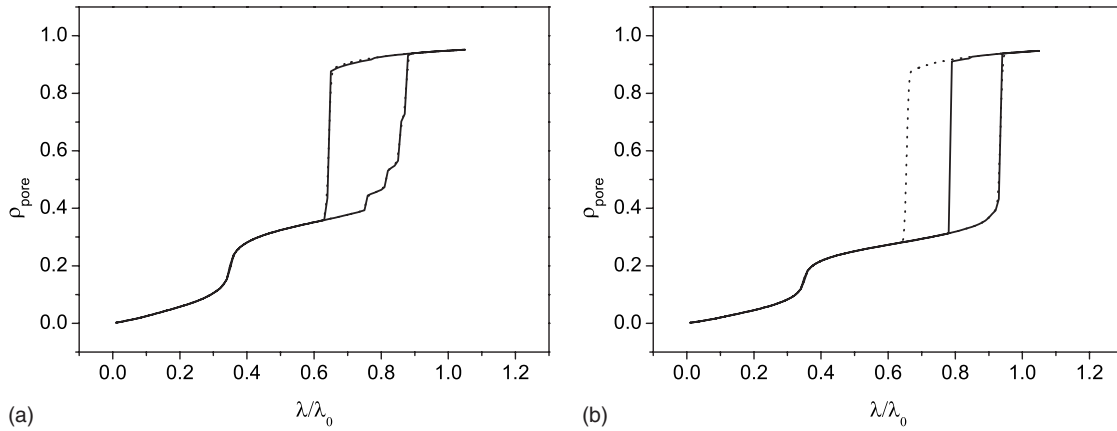
FIG. 7. Adsorption and desorption isotherms for the A- and B-type channels for the case of finite (solid line) and infinitely extended (dotted line) pores. For the infinite pore, the desorption occurs always at the limit of stability of the liquid in the pore. The desorption from the pore in contact with the bulk phase may also occur by the close to equilibrium transition [32].

geneous surfaces are presented for the case of the finite channel in contact with external gaseous phase (solid line) and the infinite channel (dotted line). As discussed in Ref. [32], the isotherms in the finite length pore and the infinite length pore are essentially indistinguishable except for the desorption branch in the hysteresis region. The desorption step from the pore in contact with the bulk phase occurs close to the equilibrium vapor-liquid transition [28,39], while the desorption in the infinite channels occurs at the limit of the stability of liquid in the pore. For the case of the type A channel, where the desorption isotherms coincide for both finite and infinite lengths, the limit of stability of the liquid in larger segments is attained prior to the condition of the evaporation from the necks created by the smallest segments, and the cavitation, i.e., formation of gas bubbles occurs. In the type B channels with wider segments, the evaporation from the smallest pore segments governs the desorption, which occurs at higher z values than the limit of stability of the liquid in the widest segments.

With increasing the mean pore size, as in the case of B-type channel [Fig. 6(b)], the adsorption behavior changes. Although the monolayer transition on the homogeneous surface occurs in the same manner as in the former case, the capillary condensation occurs in one step after a fluid film covers the surface. Thus, formation of a liquid film on the pore walls may be thought as making the effective segment size almost uniform along the entire channel. In Fig. 8, one
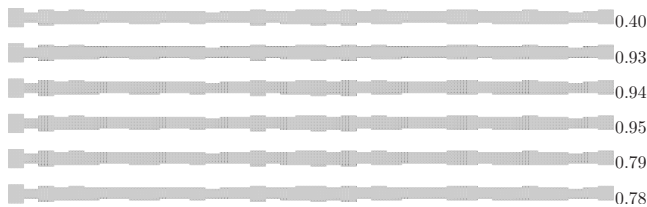
may see the adsorption step from $z=0.93$, where the mesoscopically rough surface is covered by the film of different film thickness, to $z=0.94$ where the condensation all over the channel occurs. This process creates the steep jump in the amount adsorbed in the isotherm [solid line in Fig. 6(b)]. During the desorption, the pore blocking effect dominates the emptying of the pores ($z=0.79$ to $z=0.78$). The microscopic surface roughness leads to the narrowing of the necks, thus, making the desorption due to the cavitation in wider pores occur earlier [dot-dashed line in Fig. 6(b) at $z\approx0.70$] than the evaporation from the necks, which MFT predicts to takes place at $z\approx0.63$ under given conditions.

The influence of the liquid layer, which covers the surface, becomes more significant with increasing mean pore size (Fig. 9). For the C channel with mean segment size of 10 lattice units, the formation of more liquid layers on top of the surface layer is possible, as indicated by the stepping in the adsorption isotherm in Fig. 6(c) at $z=0.92$. The pore blocking effect again governs the desorption, as observed in cases of B channel. The calculation of the desorption isotherms for the infinite length pore of type C shows similar behavior as observed in the case B [Fig. 7(b)], i.e., the condition of the evaporation from the necks on desorption is attained prior to the limit of stability of the liquid in the pore.

Widening of the PSD (case D) around the same mean value of 8 lattice units (case B) makes the cavitation in big-

FIG. 8. Visualizations of fluid density states in the B pore with homogeneous flat surface. The sequence of states corresponds to adsorption followed by desorption from top to bottom. The z values are given to the right of the images. The first 40 segments of the pore are shown with the pore opening and bulk region on the left.
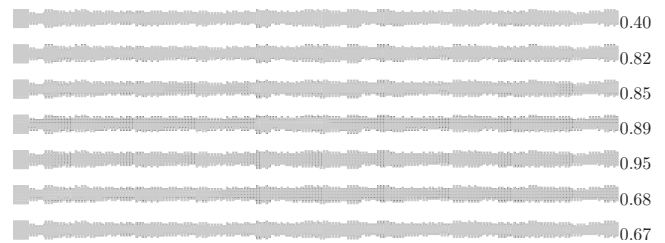
FIG. 9. Visualizations of fluid density states in the B pore with geometrical roughness. The sequence of states corresponds to adsorption followed by desorption from top to bottom. The z values are given to the right of the images. The first 40 segments of the pore are shown with the pore opening and bulk region on the left.
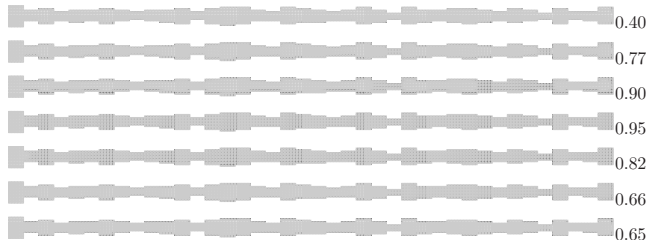
FIG. 10. Visualizations of fluid density states in the channel D with homogeneous flat surface. The sequence of states corresponds to adsorption followed by desorption from top to bottom. The z values are given to the right of the images. The first 40 segments of the pore are shown with the pore opening and bulk region on the left.

FIG. 11. Visualizations of fluid density states in the channel D with geometrical roughness. The sequence of states corresponds to adsorption followed by desorption from top to bottom. The z values are given to the right of the images. The first 40 segments of the pore are shown with the pore opening and bulk region on the left.

ger segments (e.g., with a size of 12 lattice units) possible before the evaporation condition for the necks (4 lattice units) is fulfilled. Since the volume of the neck segments is sufficiently smaller compared to the volume of the bubbles created by the cavitation, one observes a very steep decrease in the average density as indicated in Fig. 6(d) at $z \approx 0.65$. This makes the cavitation indistinguishable from the pore blocking in the desorption isotherm, but it can be recognized in the density profiles [Fig. 10]. The desorption isotherms for the finite length and infinite length D-type channel are indistinguishable, similarly to the case A [Fig. 7(a)], which supports the picture of the cavitation prior to the evaporation from the necks blocking access to the external bulk phase. In Fig. 10, one may see the smallest pore segments still filled with liquid at $z=0.65$ after the cavitation in wider pore segments proceeded.

B. Effect of surface roughness

Introducing atomistic roughness to the pore walls does not change the qualitative picture for most cases. As shown in Fig. 6 (dot-dashed line) for all channels with different PSDs studied in this work, the surface roughness smooths the layering transition due to the inhomogeneity of the surface field created by the pore wall roughness. Such a roughness does not change the mean pore size but varies the segment size locally, creating, in some cases, smaller and in some cases wider pores. In Fig. 4, some of selected fluid density profiles for A-type channel during the adsorption and desorption are presented. The wider PSD yields a gradual adsorption isotherm [Fig. 6(a)] because adsorption is now governed by the capillary condensation and the growth of liquid bridges ($z =0.75$). Similar to the flat homogeneous surface, the desorption is controlled by first stretching the liquid at $z=0.64$ (represented by the lightened color) followed by the cavitation at the limit of the mechanical stability of the liquid ($z=0.63$) and the evaporation from the remaining liquid phase. The roughness may narrow the pore segments creating very narrow necks. Thus, on the desorption, the limit of stability of the liquid in the larger pore segments may be attained earlier than the condition of the evaporation from the necks. This effect is even stronger pronounced in the case of the D-type channel, where the necks connect significantly big cavities with the external gas phase. Thus, in Fig. 11, one recognizes
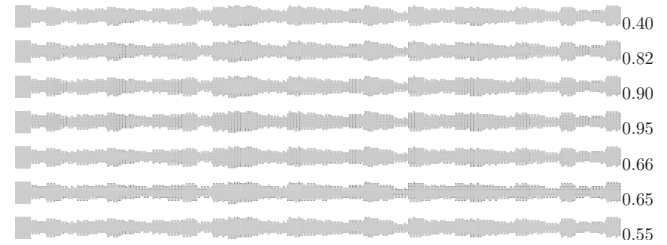
the desorption controlled by the cavitation in wider segments (step $z=0.66$ to $z=0.65$) additionally to the pore blocking.

C. Chemical heterogeneity

To study the relation between the surface roughness and the chemical heterogeneity of the surface, we have considered distribution of the surface field on the flat surface of the channels. Figure 6 shows the isotherms obtained with the surface field disorder (dashed lines). The chemical heterogeneity of the pore wall leads to the early stage adsorption behavior being very similar to that obtained with the geometrical disorder. After the surface layer is formed, the impact of the chemical heterogeneity on the next layer formation or the capillary condensation reduces. In Fig. 5, the heterogeneous adsorption on the surface leading to the continuous increase in the amount adsorbed ($z=0.18$) is observed. When the surface is covered by the liquid layer ($z =0.40$), no or minor difference in the isotherms may be observed in comparison to the flat homogeneous surface (Fig. 3).

The hysteresis loops look very similar to that for the homogeneous surface with $y=2$. In Fig. 12, the effect of different y distributions is presented for the case of A-type channel. As one may expect, the isotherms for the continuous
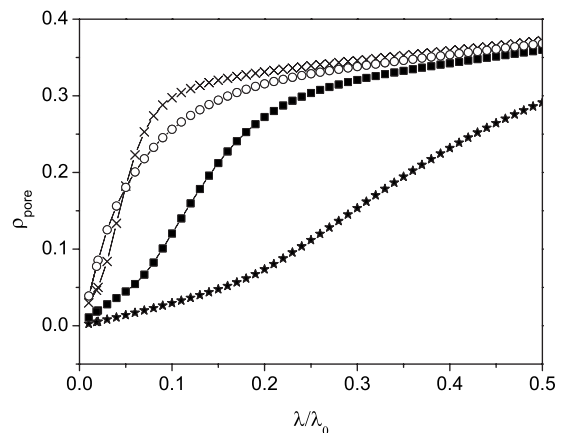
FIG. 12. Adsorption and/or desorption isotherms for the A pore with heterogeneous surface field. $1 \le y \le 3$: star symbols, $2 \le y \le 4$: square symbols, $3 \le y \le 5$: cross symbols, and $2 \le y \le 6$: circle symbols. $T^*=1$.
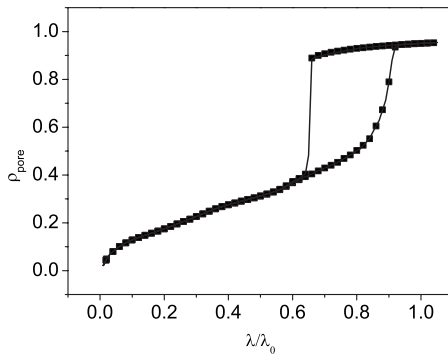
FIG. 13. Adsorption and desorption isotherms calculated for the D-type pore open at both ends (solid line) and closed at one end (square symbols).

random variation in y in the range of 1–3, 2–4, 3–5, and 2–6, respectively, show higher amount adsorbed at the same activity with increasing solid-fluid attraction strength and a dependence of the shape of the isotherms at low z on the y distribution.

As mentioned above, the impact of the chemical heterogeneity is similar to that of the roughness. The ϕ variation created according to that due to the surface roughness reproduces the low z behavior of the rough surface (Fig. 6, dashed line vs dot-dashed line).

D. Effect of pore openings

As a route to understanding the coincidence of the isotherms for the pores open at both ends and closed at one end observed in experiments [7,8], we have performed additional calculations for all channels with rough surface (see Fig. 11) closed at one end. As we have discussed before, the desorption is controlled by the cavitation and pore blocking. For the case of pore blocking effect controlling the emptying of the channel, one would expect the isotherms to coincide. Due to the random distribution of the segment sizes H_i and the sufficiently long pore, there are always narrow necks close to both pore ends. If the condition for the evaporation from these necks is fulfilled, it makes no difference whether the fluid evaporates from the wider segments over a single or over both pore openings.

Figure 13 shows the adsorption and/or desorption isotherms for the D-type channel with the pores open at both ends (solid line) and the pores closed at one end (square symbols). As observed before, in this case one observes a strong impact of the cavitation on the desorption. The most important feature of Fig. 13 is the absence of any difference between the isotherms for the channels open at both ends and closed at one end. This is in complete agreement with experiments mentioned earlier [7,8]. As has been already discussed elsewhere [24], there is little or no hysteresis in a linear pore with one end open and pronounced hysteresis for a both ends open pore, which is in agreement with Cohan [18].

E. Role of the external surface

Coasne *et al.* [7] suggested the importance of liquid layer covering the external surface of the porous film for the de-
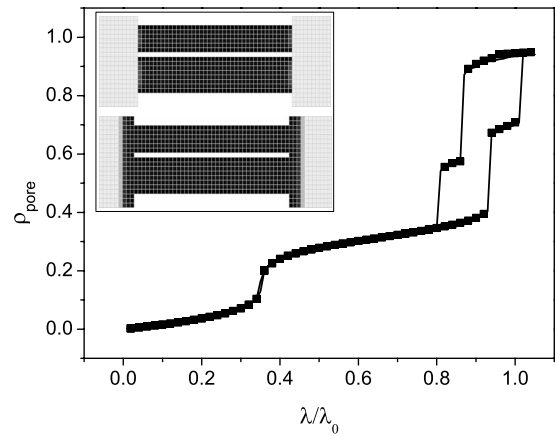
FIG. 14. Adsorption and/or desorption isotherms for two independent pores (solid line) and two pores connected via a fluid film on the substrate surface (square symbols). The visualizations of the systems show the state with completely filled pores ($y=2, T^*=1$).

sorption process in PSi materials. A similar assumption has been made in [14] to describe the shape of the adsorption hysteresis. With this in mind, we have performed studies using MFT of how the existence of the external surface layer may affect the obtained experimental results. In Fig. 14, the cumulative adsorption and/or desorption isotherms are shown for two independent slit pores (height of 6 and 8 lattice units) and two pores of same shape connected over the external surface. The inset of Fig. 14 shows the visualization of the profile density for both cases at full loading. The slight difference of the desorption isotherms are due to a small difference of the liquid-vapor meniscus shape and disappears with increasing pore length. Thus, no influence of the external surface is observed in our MFT calculations.

IV. DISCUSSION AND CONCLUSIONS

The results of our study by means of the mean-field theory applied to a gas lattice model reveal three types of disorder, which have an effect on the adsorption and/or desorption behavior at different length scales and at different sorption stages. It has been found that the chemical heterogeneity, achieved by varying the surface field of a flat pore, affects only low-pressure processes of surface adsorption. It generally smooths layering transitions at early stages of adsorption at low external activities as can be seen in Fig. 6 for all channel types studied.

After the entire surface is covered by the liquid, the capillary condensation and/or evaporation and, thus, the hysteresis loop, are almost not affected by the surface field variation. This one may note in Fig. 6 for all channel types ($z \geq 0.40$), where the isotherms for homogeneous (thin line) and chemically heterogeneous (dashed line) surfaces coincide. However, when the range of influence of the surface becomes comparable to the pore segment size H_i, some changes in the desorption behavior can be observed.

The uptake at low external activities is observed to become steeper with increasing surface field. Additionally, MFT shows that the distribution of attraction strengths plays

a significant role on the shape of the low-pressure part of adsorption isotherm (compare case $3 \leq y \leq 5$ and $2 \leq y \leq 6$ in Fig. 12).

Similar to the effect of chemical heterogeneity, the pore wall roughness produces a variation in the surface field, thus, having a strong impact on the layering transitions. In Figs. 6(a)–6(d), the isotherms for the case of surface roughness (thick solid lines) and chemical heterogeneity (dashed lines, chemical heterogeneity created to reproduce the surface field variation as exerted by the surface roughness) may be compared. The reversible adsorption and/or desorption isotherms at low z coincide until a surface layer is formed. In contrast to the chemical heterogeneity, the surface roughness produces a variation in the segment sizes, which may also influence the capillary condensation. The capillary condensation occurs first in necks followed by the growth of the liquid bridges, which is reflected by the higher amount adsorbed in Fig. 6(a). The additional necks created by the surface roughness may also have an impact on the desorption process.

In the case when the length scale of the roughness corresponds to the pore size, it may lead to cavitation in the pore segments disconnected from the external gas phase by small necks. This is observed for the type B channel, where the surface roughness creates narrow necks. It has already been observed by molecular-dynamics and Monte Carlo simulations that the mass transfer can occur through the necks filled with liquid [24,40–42]. In [24], the authors emphasize its dependence on the model parameters, pore geometry, and the temperature, which is in complete agreement with our calculations.

With increasing pore size as in the case of B- and C-type channels, one observes the desorption behavior solely controlled by the pore blocking as in the case of the smooth surface (Fig. 3). Our calculations show that without geometrical roughness, the hysteresis loop is characterized by the steep condensation jumps due to the condensation in successively wider pore segments and a sharp desorption due to pore blocking. When the surface roughness affects the PSD significantly, the hysteresis loop shows the typical asymmetry (H2 type [43]), as observed in experiments for PSi mate-rial. The decreasing influence of the wall roughness on the hysteresis loop with increasing pore size (what one may expect, e.g., for porous alumina oxide [44,45]), the hysteresis loop becomes more and more symmetric, type H1.

We should point out that in our calculations, the surface roughness corresponds to atomistic disorder. Mesoscale disorder corresponds rather to the materials with a significant pore size variation. As one may see in Fig. 6, our model calculations reveal that the main qualitative properties of the hysteresis loop are governed by the mesoscale disorder. This is in agreement with suggestions based on the experimental observations by Wallacher *et al.* [10]. An important observation is shown in Fig. 13. There is no necessity for interactions between the neighboring channels, as suggested in some recent papers [13,14,46], for these materials to exhibit H2 hysteresis.

To conclude, in the present work, we have studied the influence of the geometrical and chemical disorder in linear pores upon the adsorption and/or desorption behavior using MFT. The model systems studied here capture the main adsorption and/or desorption properties of electrochemically etched porous silicon. In contrast to the analogous template-based materials with smoother channel-like pores such as SBA-15, MCM-41, or anodic aluminum oxide, mesoporous silicon has similar adsorption properties to that of disordered materials with a network of mesopores (e.g., porous glasses). Our model results suggest that these properties (asymmetric hysteresis of type H2, insensitivity of the results to pore closure at one end) can be uniformly explained assuming a distribution of pore diameter together with surface roughness. In this sense, linear pores with statistically varying pore diameter and surface roughness exhibit adsorption and/or desorption properties similar to those of three-dimensional pore networks.

[1] D. Everett, Trans. Faraday Soc. **50**, 1077 (1954).

[2] K. Sing, D. Everett, R. Haul, L. Moscou, R. Pierotti, J. Rouquerol, and T. Siemieniewska, Pure Appl. Chem. **57**, 603 (1985).

[3] G. Mason, Proc. R. Soc. London, Ser. A **390**, 47 (1983).

[4] L. D. Gelb, K. E. Gubbins, R. Radhakrishnan, and M. Sliwinska-Bartkowiak, Rep. Prog. Phys. **62**, 1573 (1999).

[5] S. Naumov, R. Valiullin, J. Kärger, R. Pitchumani, and M.-O. Coppens, Microporous Mesoporous Mater. **110**, 37 (2008).

[6] A. Cullis, L. Canham, and P. Calcott, J. Appl. Phys. **82**, 909 (1997).

[7] B. Coasne, A. Grosman, C. Ortega, and M. Simon, Phys. Rev. Lett. **88**, 256102 (2002).

[8] S. Naumov, A. Khokhlov, R. Valiullin, J. Kärger, and P. A. Monson, Phys. Rev. E **78**, 060601 (2008).

[9] S. Uehara, K. Taira, T. Hashimoto, H. Sasabu, and T. Matsubara, Phys. Status Solidi A **182**, 443 (2000).

[10] D. Wallacher, N. Künzner, D. Kovalev, N. Knorr, and K. Knorr, Phys. Rev. Lett. **92**, 195704 (2004).

[11] A. Khokhlov, R. Valiullin, J. Kärger, F. Steinbach, and A. Feldhoff, New J. Phys. **9**, 272 (2007).

[12] B. Coasne, A. Grosman, N. Dupont-Pavlovsky, C. Ortega, and M. Simon, Phys. Chem. Chem. Phys. **3**, 1196 (2001).

[13] A. Grosman and C. Ortega, Langmuir **21**, 10515 (2005).

[14] A. Grosman and C. Ortega, Langmuir **24**, 3977 (2008).

[15] A. V. Kityk, T. Hofmann, and K. Knorr, Phys. Rev. Lett. **100**, 036105 (2008).

[16] S. Gruener and P. Huber, Phys. Rev. Lett. **100**, 064502 (2008).

[17] A. V. Kityk, M. Wolff, K. Knorr, D. Morineau, R. Lefort, and P. Huber, Phys. Rev. Lett. **101**, 187801 (2008).

[18] L. H. Cohan, J. Am. Chem. Soc. **60**, 433 (1938).

[19] B. Coasne, A. Grosman, C. Ortega, and R. J. M. Pellenq, Characterization Porous Solids VI **144**, 35 (2002).

[20] E. Kierlik, P. Monson, M. Rosinberg, L. Sarkisov, and G. Tarjus, Phys. Rev. Lett. **87**, 055701 (2001).

[21] H.-J. Woo and P. A. Monson, Phys. Rev. E **67**, 041207 (2003).

[22] D. Everett and W. Whitton, Trans. Faraday Soc. **48**, 749 (1952).

[23] D. Everett and F. Smith, Trans. Faraday Soc. **50**, 187 (1954).

[24] B. Libby and P. Monson, Langmuir **20**, 4289 (2004).

[25] P. I. Ravikovitch and A. V. Neimark, Langmuir **18**, 9830 (2002).

[26] M. Thommes, B. Smarsly, M. Groenewolt, P. I. Ravikovitch, and A. V. Neimark, Langmuir **22**, 756 (2006).

[27] M. Deoliveira and R. Griffiths, Surf. Sci. **71**, 687 (1978).

[28] U. M. Marconi and F. Van Swol, Phys. Rev. A **39**, 4109 (1989).

[29] R. Evans, U. Marconi, and P. Tarazona, J. Chem. Soc. **82**, 1763 (1986).

[30] E. Kierlik, M. Rosinberg, G. Tarjus, and E. Pitard, Mol. Phys. **95**, 341 (1998).

[31] H. Woo, L. Sarkisov, and P. Monson, Langmuir **17**, 7472 (2001).

[32] P. Monson, J. Chem. Phys. **128**, 084701 (2008).

[33] P. A. Monson, Langmuir **24**, 12295 (2008).

[34] L. Gelb, Mol. Phys. **100**, 2049 (2002).

[35] L. Sarkisov and P. A. Monson, Phys. Rev. E **65**, 011202 (2001).

[36] E. O. Kraemer, *A Treatise on Physical Chemistry*, edited by H. S. Taylor (Van Nostrand, New York, 1931).

[37] J. W. McBain, J. Am. Chem. Soc. **57**, 699 (1935).

[38] D. Everett, *The Solid-Gas Interface* (Dekker, New York, 1967), Vol. 2.

[39] P. C. Ball and R. Evans, Langmuir **5**, 714 (1989).

[40] L. Sarkisov and P. Monson, Langmuir **17**, 7600 (2001).

[41] P. Ravikovitch and A. Neimark, Langmuir **18**, 1550 (2002).

[42] H.-J. Woo, F. Porcheron, and P. A. Monson, Langmuir **20**, 4743 (2004).

[43] K. S. Sing and R. T. Williams, Adsorpt. Sci. Technol. **22**, 773 (2004).

[44] F. Casanova, C. E. Chiang, C.-P. Li, and I. K. Schuller, Appl. Phys. Lett. **91**, 243103 (2007).

[45] L. Bruschi, G. Fois, G. Mistura, K. Sklarek, R. Hillebrand, M. Steinhart, and U. Gösele, Langmuir **24**, 10936 (2008).

[46] Annie Grosman and Camille Ortega, Phys. Rev. B **78**, 085433 (2008).